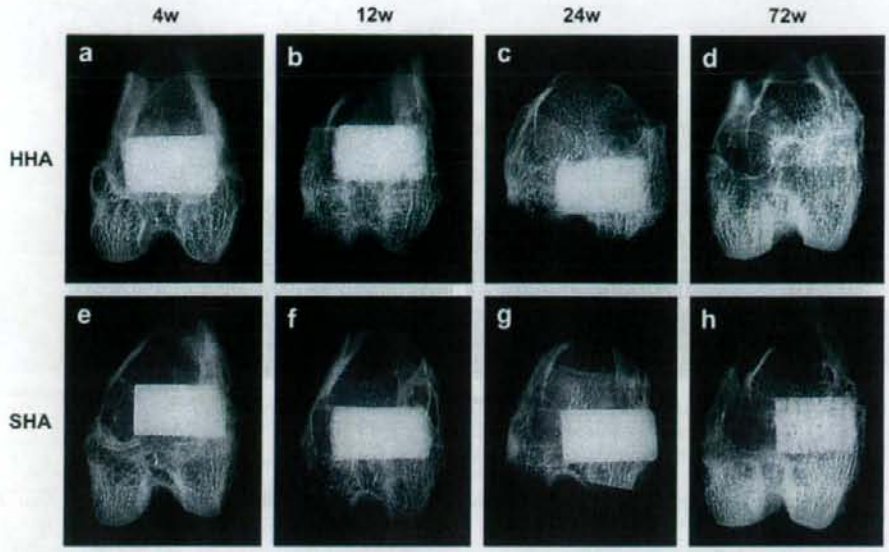

Fig. 3. Soft X-ray photographs of the operated portion of the rabbit femur. Four weeks (a), 12 weeks (b), 24 weeks (c) and 72 weeks (d) after implantation of HHA, 4 weeks (e), 12 weeks (f), 24 weeks (g) and 72 weeks (h) after implantation of SHA. Involvement of HHA in bone tissue was evident at 72 weeks (h).

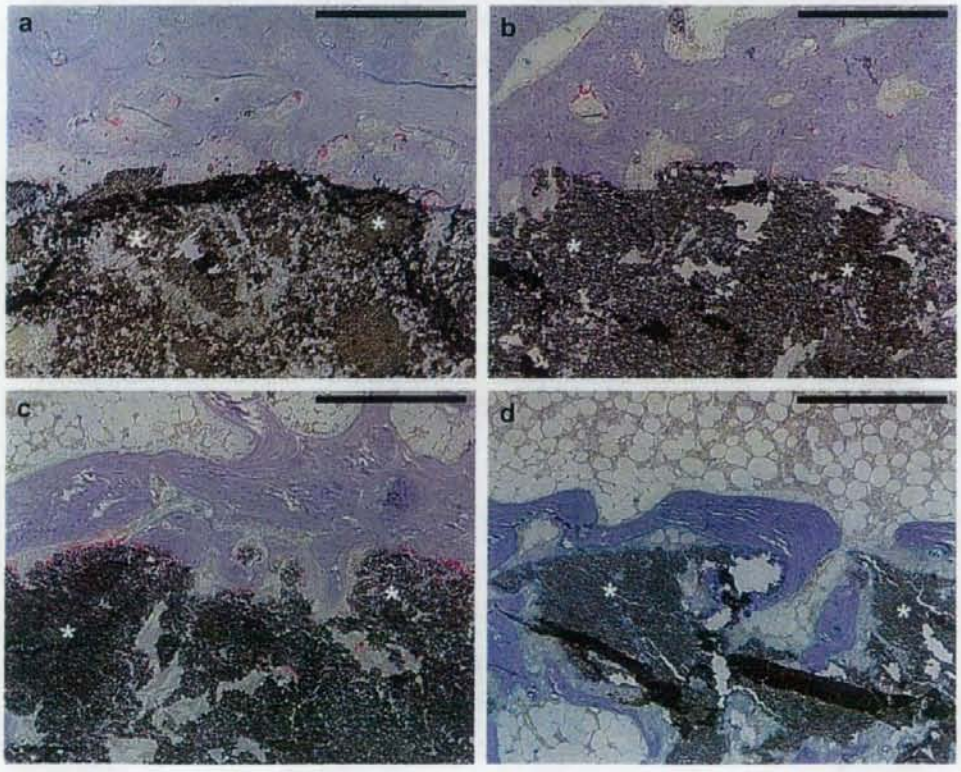

Fig. 4. Histological appearance of specimens implanted with HHA. Two weeks (a), 4 weeks (b), 12 weeks (c), and 24 weeks (d) after the operation. Sections were stained for TRAP activity. Asterisks (*) represent the implanted bone substitute. Bar: (a)–(d) 500 μm.

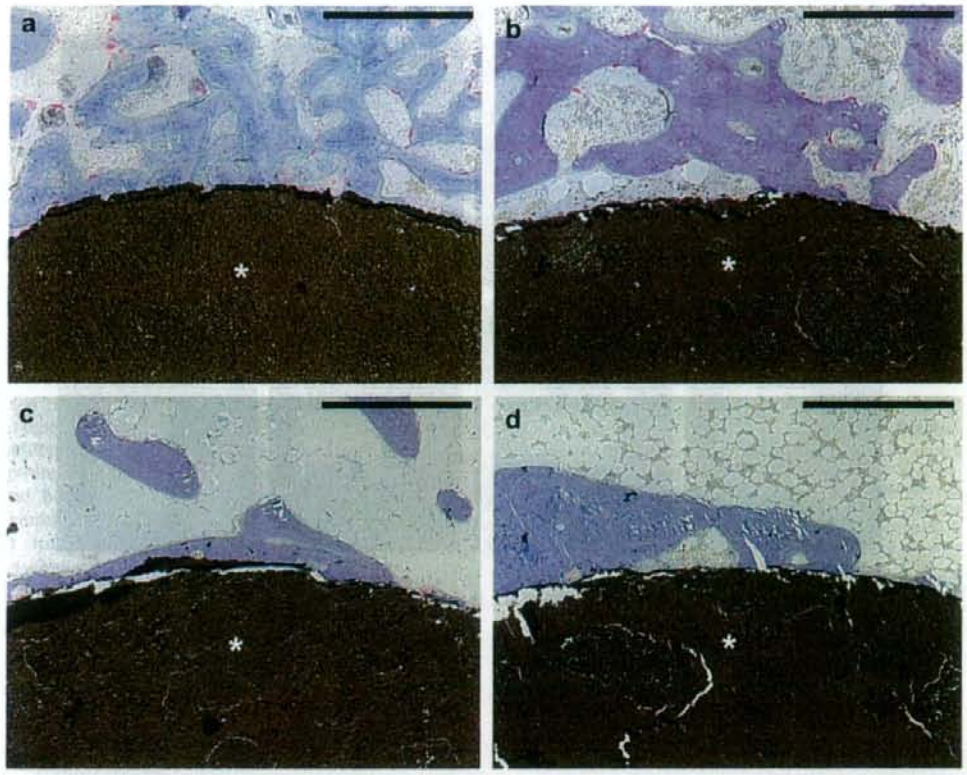

Fig. 5. Histological appearance of specimens implanted with SHA. Two weeks (a), 4 weeks (b), 12 weeks (c), and 24 weeks (d) after the operation. Sections were stained for TRAP activity. Asterisks (*) represent the implanted bone substitute. Bar: (a)–(d) 500 μm.

2.3. Radiological and histological analyses

The distal portion of the left femur was dissected from the sacrificed animals, and X-ray photographs were taken using a soft X-ray apparatus (TRS-1005, SOFRON, Tokyo, Japan). All the harvested tissue specimens were fixed in 4% formaldehyde in 0.1 M phosphate buffer (pH 7.2), embedded in 2-hydroxyethyl methacrylate/methyl methacrylate/2-hydroxyethyl acrylate mixed resin, and sectioned 3 μm thick [4]. These sections were stained with toluidine blue or histochemically stained for tartrate-resistant acid phosphatase (TRAP) activity as described previously [15].

2.4. Histomorphometry

Histomorphometric analyses were performed using the Osteoplan II system (Carl Zeiss, Thornwood, NY) as described previously [16]. Bone volume/tissue volume (BV/TV, %), bone formation rate/bone surface (BFR/BS, $mcm^3/mcm^2/d$), mineral apposition rate (MAR, mcm/d), number of osteoclasts/bone perimeter (N.Oc/B.Pm, per 100 mm), and osteoclast surface/bone surface (Oc.S/BS, %) were calculated for each sample in four squares (0.4 mm × 1.2 mm), each of which was arranged adjacent to two squares with shorter sides of 1.2 mm long, which inscribed proximodistally and antero-posteriorly in a circle of the implant 6 mm in diameter. An

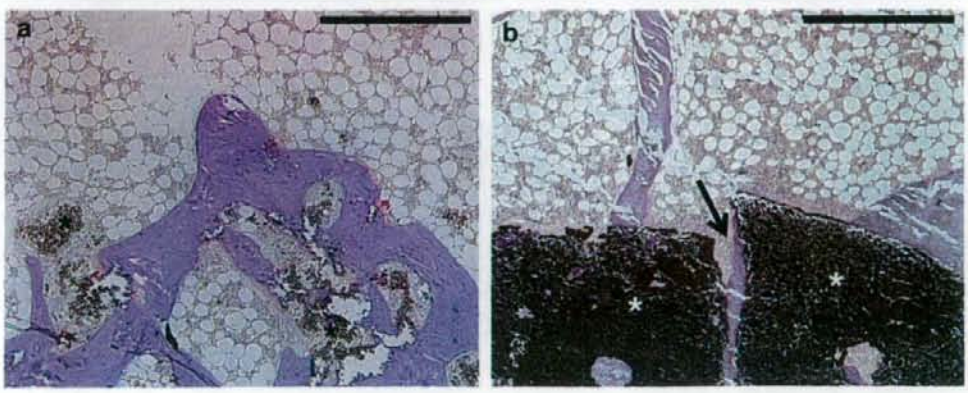

Fig. 6. Comparison of histological appearance of specimens 72 weeks after implantation of HHA and SHA. Implantation of HHA (a) and SHA (b). Sections were stained for TRAP activity. A crack in SHA with newly formed bone tissue (an arrow) was evident (b). Asterisks (*) represent the implanted bone substitute. Bar: (a) and (b) 500 μm.

osteoclast was defined as a multinucleated cell in contact with the surface of a bone or bone substitute. MAR was calculated under a fluorescence microscope at a wavelength of 455 nm. To calculate BV/TV, N.Oc/B.Pm, Oc.S/BS, and BFR/BS, sections stained with toluidine blue were used. Statistical differences were evaluated using the *t*-test.

2.5. In vitro experiments

Osteoblasts were generated using C2C12 preosteoblastic cells with stimulation of recombinant human bone morphogenetic protein-2 (Pepro Tech Inc., Rocky Hill, NJ) at a concentration of 300 ng/ml in α-minimal essential medium supplemented with 10% fetal bovine serum. The procedure followed previous reports [17]. The discs used for the experiment were fixed with methanol/acetone (6:4) fixative, and stained for alkaline phosphatase (ALP) activity on the 6th day of culture.

Osteoclasts were generated using mouse bone marrow macrophages prepared from the femora and tibiae of 5-week-old female ddY mice and recombinant soluble isoform of mouse receptor activator of nuclear factor-κB ligand (RANKL) [15,18]. Bone marrow macrophages (4×10^4 cells/well) were seeded in 48-well plates in which an HHA or SHA disc, 8 mm in diameter, was inserted per well and maintained with culture medium supplemented with 10% fetal calf serum, 30 ng/ml of mouse macrophage colony stimulating factor (M-CSF) (Sigma, St. Louis, MO) and 200 ng/ml of recombinant mouse RANKL synthesized using GST system (Amersham Pharmacia Biotech Inc., Piscataway, NJ) as reported previously [18]. All ceramic discs were presoaked in α-minimal essential medium supplemented with 10% fetal calf serum for 4 weeks, changing the culture medium every week before being used for experiments. The medium of the cultures was changed every other day. The discs used for the experiment were fixed with methanol/acetone (6:4) fixative, and stained for TRAP activity on the 8th day of culture. To analyze the viability of the cultures, the discs used for the experiment were fixed with the same fixative described above and stained the nuclei with DAPI (Dojindo Laboratories, Kumamoto, Japan). The stained nuclei were viewed under a fluorescence microscope at a wavelength of 455 nm.

3. Results

3.1. General features of samples

Synthesized HHA and SHA were analyzed by powder X-ray diffractometry with graphite-monochromatized CuKα radiation, operating at 40 kV and 20 mA (XRD; Multi Flex, Rigaku, Tokyo, Japan). No phase other than HA was detected for HHA, which was hydrothermally synthesized at 200 °C for 5 h and SHA, which was synthesized by sintering at 1100 °C (Fig. 1a,b). These results showed that both HHA and SHA were pure and uniform HA. When HHA was sintered at 900 °C, decomposition of HA to β-TCP was detected because the HHA was nonstoichiometric HA of calcium-deficient composition. There was no decomposition as a result of sintering in the case of SHA because SHA was stoichiometric (data not shown). The results corresponded to chemical analysis by ICP-MS (Seiko Inst., SPQ9000S, Japan). The surface of HHA and SHA was analyzed by scanning electron microscope (JSM-T300, JEOL, Tokyo, Japan). Pore volume and distribution of pore diameter were measured by mercury intrusion porosimetry (MIP; Carlo Elba, Porosimeter 2000, Italy). HHA was composed of rod-shaped particles about 20 μm in length, which were tangled together to form micropores about 0.2 μm in size (Fig. 2a). SHA was composed of globular particles, which fused to one another and formed micropores about 0.5 μm in size (Fig. 2b). The porosity of HHA and SHA was 70%.

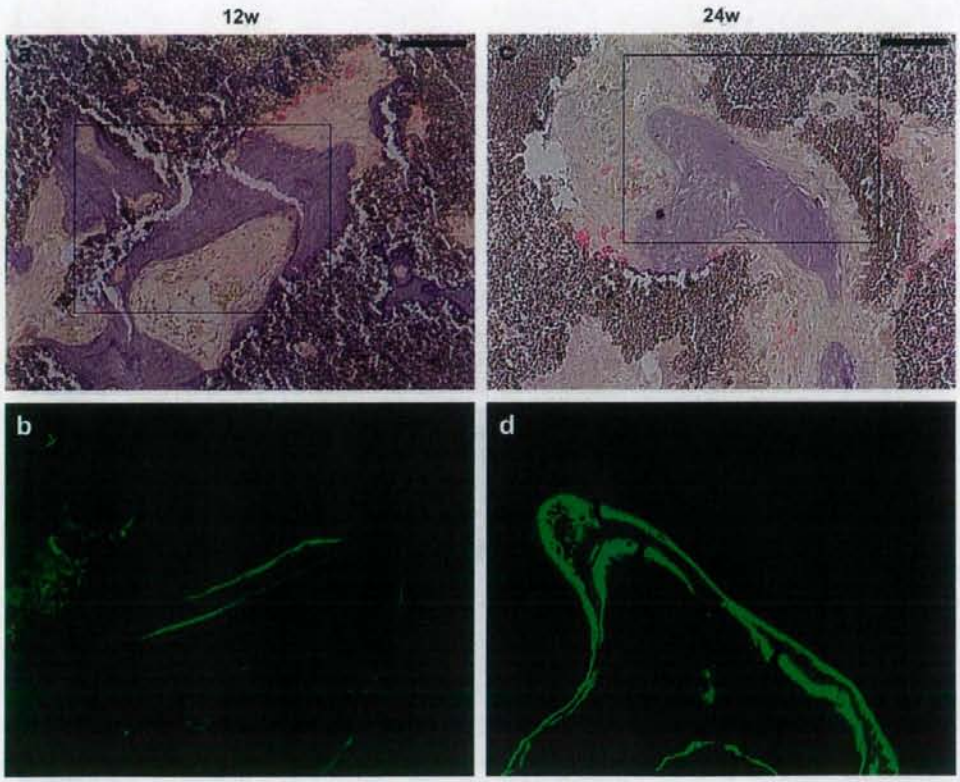

Fig. 7. Evaluation of osteogenesis in a specimen implanted with HHA by fluorescent labeling. (a,c) Bright-field light microscopic appearance of specimens 12 weeks (a) and 24 weeks (c) after HHA implantation. Sections were stained for TRAP activity. The rectangles represent the area used for fluorescent analysis. (b,d) The calcein signal in newly formed bone tissue in the specimens 12 weeks (b) and 24 weeks (d) after HHA implantation. Sections stained with toluidine blue were utilized for analysis by fluorescence microscopy. Bar: (a,c) 100 μm.

3.2. Radiological and histological analyses

Fig. 3 represents radiographs of rabbit femurs 4, 12, 24 and 72 weeks after the operation. At 4 weeks post-surgery, the implanted HHA was recognized clearly by its amorphous radiopacity on X-ray film, and no difference from the finding of SHA was seen (Fig. 3a,e). At 12 weeks, radiopacity derived from HHA was evident, but the margin was a little unclear compared to the finding of SHA (Fig. 3b,f). At 24 weeks, no difference in amorphous radiopacity of the implanted HHA was seen compared to the radiopacity at 12 weeks post-surgery (Fig. 3b,c). In radiographic appearance, the radiopacity of implanted SHA was similar from 2 to 24 weeks after the operation (Fig. 3e–g). Seventy-two weeks after the operation, the area of HHA implantation was not evident (Fig. 3d). The radiopacity of SHA was similar to those in earlier stages, but slight irregularity of the marginal region and enlargement of macropores were seen (Fig. 3h).

Histological analyses were conducted using plastic-embedded undecalcified sections stained for TRAP activity or sections stained with toluidine blue. Two weeks after the implantation of HHA, TRAP-positive osteoclasts were seen on the surface of the implant. Part of the implant directly contacted with bone (Fig. 4a). Four weeks after implantation of HHA, the histological features were similar to those at 2 weeks. Bone tissue in contact with HHA and TRAP-positive cells in contact with HHA were seen (Fig. 4b). Twelve weeks after the operation, the invasion of newly formed bone tissue into HHA implants was evident and many osteoclasts in contact with newly formed bone or HHA were seen (Fig. 4c). Twenty-four weeks after the operation, a considerable amount of HHA remained; however, the amount of newly formed bone invading the implant had increased compared with at 12 weeks (Fig. 4c,d). Infiltration of TRAP-positive osteoclasts was still evident (Fig. 4d). No evidence of bioresorption of the SHA implant was seen from 2 to 24 weeks after the operation (Fig. 5a–d). TRAP-positive osteoclasts were seen on the surface of the implant from 2 to 24 weeks after the operation, but there were fewer than those in contact with HHA.

At 72 weeks post-operation, most HHA was resorbed and substituted with newly formed bone tissue (Fig. 6a). Invasion of bone tissue into the cracked SHA implant was seen in some portions, and TRAP-positive osteoclasts were seen in these regions. Some osteoclasts contacted with SHA, but no evidence of osteoclastic resorption was seen (Fig. 6b).

3.3. Histomorphometry

Histomorphometric quantitation revealed that BV/TV in specimens implanted with HHA was significantly greater than that in specimens implanted with SHA 24 weeks after the operation (Fig. 10a). The fluorescent signal derived from calcein labeling was analyzed using a fluorescence microscope in the specimens 12 and 24 weeks after the implantation of either HHA or SHA. The width of double labeling was greater in specimens implanted with HHA than in those implanted with SHA at 12 weeks post-operation (Figs. 7b

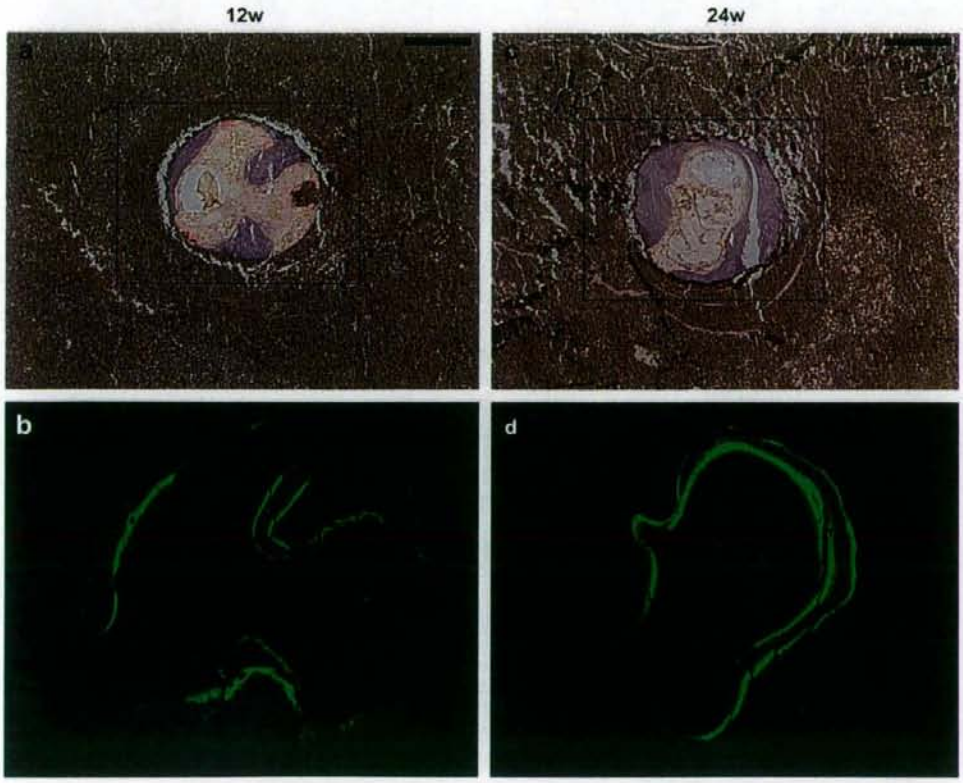

Fig. 8. Evaluation of osteogenesis in a specimen implanted with SHA by fluorescent labeling. (a,c) Bright-field light microscopic appearance of specimens 12 weeks (a) and 24 weeks (c) after SHA implantation. Sections were stained for TRAP activity. The rectangles represent the area used for fluorescent analysis. (b,d) The calcein signal in newly formed bone tissue in the specimens 12 weeks (b) and 24 weeks (d) after SHA implantation. Sections stained with toluidine blue were utilized for analysis by fluorescence microscopy. Bar: (a,c) 100 μm.

and 8b), but was not clear at 24 weeks post-operation (Figs. 7d and 8d). MAR and BFR/BS for newly formed bone tissue in each sample were quantified by histomorphometry. MAR was significantly increased in specimens implanted with HHA in comparison to specimens implanted with SHA at 12 and 24 weeks post-operation (Figs. 9b and 10b). BFR/BS revealed a strong tendency to increase in specimens implanted with HHA as compared with specimens implanted with SHA at 12 and 24 weeks after the operation (Figs. 9c and 10c). Additionally, N.Oc/B.Pm and Oc.S/BS were quantified and both were significantly increased in specimens implanted with HHA compared with those implanted with SHA at 12 and 24 weeks after the operation (Figs. 9d,e and 10d,e).

3.4. *In vitro analyses of differentiation of osteoblasts and osteoclasts*

Osteoblastic differentiation on HHA and SHA discs was analyzed using C2C12 preosteoblastic cells stimulated with recombinant human BMP-2. When C2C12 cells were cultured in medium supplemented with BMP-2 on an HHA or SHA disc, alkaline phosphatase activity was detected similarly in cells cultured on HHA and SHA discs (Fig. 11a,b). Additionally, mouse bone marrow macrophages were cultured in medium supplemented with recombinant mouse RANKL and M-CSF on discs made with HHA or SHA. Higher TRAP activity was detected in osteoclasts formed on the HHA disc than that in osteoclasts formed on the SHA disc (Fig. 11c,d). To analyze the cause of higher TRAP activity on the HHA disc, the density of cultured cells on the discs was analyzed by nuclear staining with DAPI. The density of DAPI-positive viable nuclei on HHA and SHA discs was similar (Fig. 11e,f).

4. Discussion

In this study, we confirmed that SHA was non-biodegradable in bone tissue. Throughout the experimental period, TRAP-positive osteoclasts were detected on the surface of SHA, but no evidence of osteoclastic resorption was seen (Figs. 5 and 6b). These data suggested that SHA had the potential to be recognized, but was unable to be resorbed by osteoclasts in bone. We previously showed that calcium concentration did not increase at all in the culture media of SHA, in which many osteoclasts were induced by RANKL-expressing cells [4]. Previous data also suggested that osteoclasts could not resorb SHA.

We showed that HHA had been well-recognized by osteoclasts for a long period after implantation, and mild biodegradability and good substitution for newly formed bone were detected in animal experiments. Previously, calcium-deficient HA was introduced in biological analyses [19], but the XRD pattern was not shown and the purity and uniformity of the material were uncertain. XRD of HHA showed that HHA was pure calcium-deficient HA (Fig. 1) and was composed of uniform rod-shaped particles (Fig. 2). Biodegradation of HHA by osteoclasts during the experimental period showed that molar ratio of Ca/P directly affected osteoclast activity, even though the organic components in bone tissue might also affect osteoclast activity. Biodegradation of HHA was very slow (Fig. 4), but most part of HHA was replaced by newly formed bone up to 72 weeks

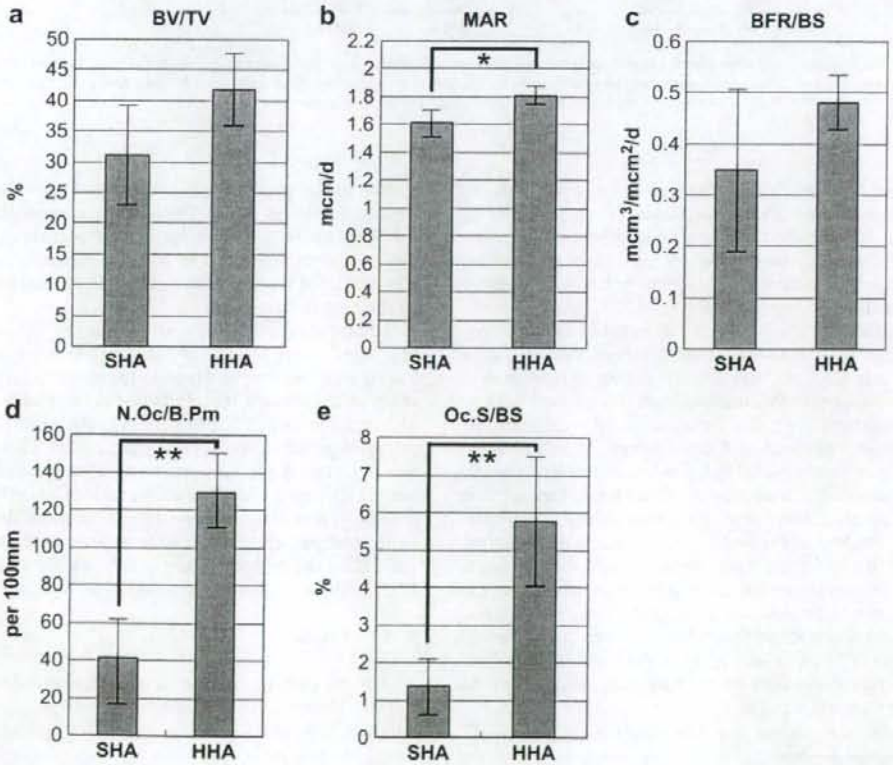

Fig. 9. Histomorphometry of newly formed bone tissue in the specimens 12 weeks after implantation. Parameters for the amount of bone, BV/TV (a), osteogenic activity, MAR (b) and BFR/BS (c), were compared between specimens implanted with HHA and specimens implanted with SHA. Parameters for bone resorption, N.Oc/B.Pm (d) and Oc.S/BS (e) were also compared (*$P < 0.05$, **$P < 0.01$). Three areas in the four samples were analyzed for the data acquired.

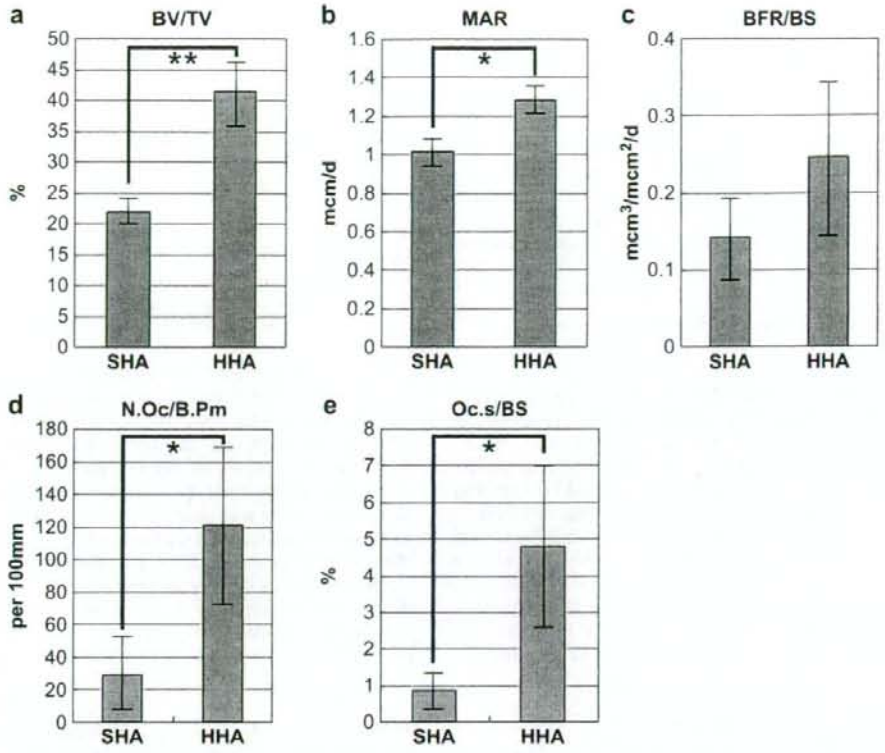

Fig. 10. Histomorphometry of the newly formed bone tissue in the specimens 24 weeks after implantation. Parameters for the amount of bone, BV/TV (a), osteogenic activity, MAR (b) and BFR/BS (c), were compared between specimens implanted with HHA and specimens implanted with SHA. Parameters for bone resorption, N.Oc/B.Pm (d) and Oc.S/BS (e) were also compared ($^{*}P < 0.05$, $^{**}P < 0.01$). Three areas in the four samples were analyzed for the data acquired.

after implantation (Fig. 6a). These data suggested that the solubility of bone substitute did not always correlated to replaceability by bone tissue. We hypothesized that if a bone substitute was continuously recognized and resorbed by osteoclasts, continuous resorption would lead to replacement by new bone tissue irrespective of the mild solubility.

Osteoblast activity in the implanted region of HHA was suggested to be higher than that of SHA from histomorphometric data, which showed that MAR was significantly higher in HHA than in SHA at 12 and 24 weeks after implantation. Considered with in vitro studies, which showed that osteoblastic differentiation occurred similarly on HHA and SHA discs, excess bone formation found in animals implanted with HHA was thought to be caused by indirect stimulation of osteoblasts by HHA. Bone formation is thought to be coupled with bone resorption in that osteoblasts express one of the key molecules for osteoclastogenesis, RANKL [20]. Conversely, the biological mechanism to stimulate osteoblasts by osteoclasts remains uncertain, but the biodegradable nature of HHA was suggested to be associated with the excess bone formation found in animals implanted with HHA. In vitro study showed higher TRAP activity of osteoclasts on HHA than that of osteoclasts on SHA, and active osteoclasts in animals implanted with HHA might influence osteoblast activity.

Previously, we have shown that the microstructure of β-TCP affected the biological response [4,21]. It is conceivable that the microstructure of HA also affects the biological response. As shown in Fig. 2a, HHA was formed by rod-shaped particles just like β-TCP composed of rod-shaped particles, which was prepared by applied hydrothermal process. β-TCP composed of rod-shaped particles showed mild and stable degradability compared to conventional β-TCP composed of globular-shaped particles, and rod-shaped particles were suggested to affect the activity of bone cells and metabolism of subsequently formed bone tissue [4]. This might also be the case in HHA.

Additionally, HHA is composed of hexagonal monocrystals with prolonged *c*-axis and the surface of HHA is suggested to be electrically charged. Previous reports suggested that the surface charge of ceramics affected the affinity or activity of bone cells [22,23]. Although the surface charge of HHA has not been directly measured yet, preferential affinity for acidic protein compared to basic protein was detected at pH 7.2 using bovine serum albumin as an acidic protein and lysozyme chloride as a basic protein [24]. Acidic protein is negatively charged in neutral conditions, and HHA was suggested to be positively charged from the experiments. Surface charge derived from the microstructure of HHA and/or attached proteins on HHA might also influence the biological behavior.

5. Conclusion

The biological response of hydrothermally synthesized pure calcium-deficient HA composed of rod-shaped particles (HHA) was different from that of stoichiometric HA synthesized by the sintering method (SHA). HHA but not SHA revealed a biodegradable nature by osteoclastic resorption. Irrespective of mild biodegradation, HHA showed good replaceability with bone tissue. Excess bone formation found in animals implanted with HHA

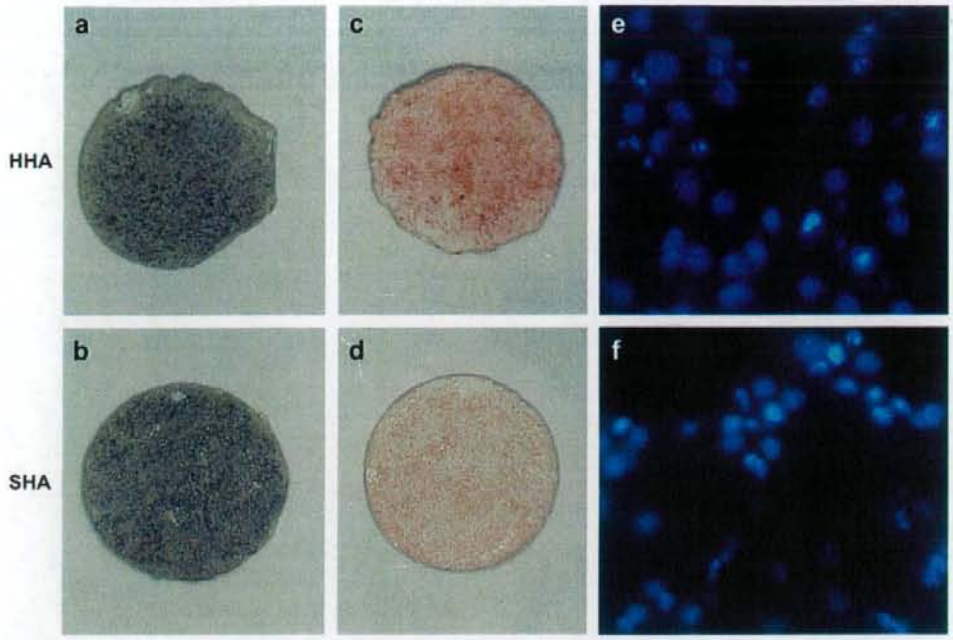

Fig. 11. The in vitro induction assay of osteoblasts and osteoclasts on HHA and SHA discs. (a,b) Alkaline phosphatase-positive C2C12 cells on HHA (a) and SHA (b) discs. (c,d) TRAP-positive bone marrow macrophages induced by recombinant RANKL on HHA (c) and SHA (d) discs. (e,f) Nuclear appearances of bone marrow macrophages cultured on HHA (e) and SHA (f) discs stained with DAPI.

compared with those implanted with SHA was suggested to be associated with the biodegradability of HHA. The method to synthesize biodegradable pure calcium-deficient HA is expected to contribute to developing new biodegradable bone substitutes with adequate biodegradability and bone replaceability.

Acknowledgments

We thank Drs. T. Sawase and D. Ono of the Department of Fixed Prosthodontics and Oral Rehabilitation, Nagasaki University Graduate School of Biomedical Sciences for technical assistance and discussion, and Mr. Takaharu Tsukada of the Department of Experimental Surgery and Biomedical Resources, Juntendo University School of Medicine and Kitayama Labes Co. Ltd. for technical consultations on the animal experiments. This work was supported by a Grant-in-Aid from the ministry of Education, Culture, Sports, Science, and Technology of Japan (Grant nos. 18390519 and 18659541) and "Ground-based Research Program for Space Utilization" promoted by Japan Space Forum.

References

[1] Toya H, Ito A, Fujimori H, Goto S, Ioku K. In vitro estimation of calcium phosphate with pH-controlled simulated body fluid. Trans Mater Res Soc Jpn 2001;26:1247–50.
[2] Ioku K, Misumi H, Fujimori H, Goto S. Porous β-tricalcium phosphate ceramics of bimodal pore size distribution. Trans Mater Res Soc Jpn 2003;28:781–4.
[3] Ioku K, Kawachi G, Nakahara K, Ishida EH, Minagi H, Okuda T, et al. Porous granules of β-tricalcium phosphate composed of rod-shaped particles. Key Eng Mater 2006;309–311:1059–62.
[4] Okuda T, Ioku K, Yonezawa I, Minagi H, Kawachi G, Gonda Y, et al. The effect of the microstructure of β-tricalcium phosphate on the metabolism of subsequently formed bone tissue. Biomaterials 2007;28:2612–21.
[5] Bucholz RW, Carlton A, Holmes R. Interporous hydroxyapatite as a bone graft substitute in tibial plateau fractures. Clin Orthop Relat Res 1989;240:53–62.
[6] Hoogendoorn HA, Renooij W, Akkermans LM, Visser W, Wittebol P. Long-term study of large ceramic implants (porous hydroxyapatite) in dog femora. Clin Orthop Relat Res 1984;187:281–8.
[7] LeGeros RZ. Properties of osteoconductive biomaterials: calcium phosphates. Clin Orthop Relat Res 2002;395:81–98.
[8] LeGeros R. Biological and synthetic apatite. In: Broen PW, Constaqntz B, editors. Hydroxyapatite and related materials. CRC Press; 1994. p. 3–28.
[9] Kim HM, Rey C, Glimcher MJ. Isolation of calcium-phosphate crystals of bone by non-aqueous methods at low temperature. J Bone Miner Res 1995;10:1589–601.
[10] Ioku K, Kawachi G, Yamasaki M, Toda H, Fujimori H, Goto S. Hydrothermal preparation of porous hydroxyapatite with tailrod crystal surface. Key Eng Mater 2005;288–289:521–4.
[11] Ioku K, Kawachi G, Sasaki S, Fujimori H, Goto S. Hydrothermal preparation of tailrod hydroxyapatite. J Mater Sci 2006;41:1341–4.
[12] Yoshimura M, Suda H, Okamoto K, Ioku K. Hydrothermal synthesis of biocompatible whiskers. J Mater Sci 1994;29:3399–402.
[13] Ioku K, Nishimura S, Eguchi Y, Goto S. Hydrothermal preparation of porous hydroxyapatite ceramics. Rev High Pressure Sci Technol 1998;7:1398–400.
[14] Ioku K, Misumi H, Fujimori H, Goto S, Yoshimura M. Porous ceramics of calcium phosphates prepared by hydrothermal method. In: Re R, editor. Proceedings of the 5th international conference on solvo-thermal reactions, 2002, USA; 2002. p. 233–6.
[15] Ikeda T, Kasai M, Suzuki J, Kuroyama H, Seki S, Utsuyama M, et al. Multimerization of the receptor activator of nuclear factor-kappaB ligand (RANKL) isoforms and regulation of osteoclastogenesis. J Biol Chem 2003 Nov 21;278(47):47217–22.
[16] Parfitt AM, Drezner MK, Glorieux FH, Kanis JA, Malluche H, Meunier PJ, et al. Bone histomorphometry: standardization of nomenclature, symbols, and units. Report of the ASBMR Histomorphometry Nomenclature Committee. J Bone Miner Res 1987;2:595–610.
[17] Zhao B, Katagiri T, Toyoda H, Takada T, Yanai T, Fukuda T, et al. Heparin potentiates the in vivo ectopic bone formation induced by bone morphogenetic protein-2. J Biol Chem 2006;281:23246–53.
[18] Suzuki J, Ikeda T, Kuroyama H, Seki S, Kasai M, Utsuyama M, et al. Regulation of osteoclastogenesis by three human RANKL isoforms expressed in NIH3T3 cells. Biochem Biophys Res Commun 2004;314:1021–7.
[19] Kasten P, Vogel J, Luginbuhl R, Niemeyer P, Tonak M, Lorenz H, et al. Ectopic bone formation associated with mesenchymal stem cells in a resorbable calcium deficient hydroxyapatite carrier. Biomaterials 2005;26:5879–89.
[20] Suda T, Takahashi N, Udagawa N, Jimi E, Gillespie MT, Martin TJ. Modulation of osteoclast differentiation and function by the new members of the tumor necrosis factor receptor and ligand families. Endocr Rev 1999;20:345–57.

[21] Yokozeki H, Hayashi T, Nakagawa T, Kurosawa H, Shibuya K, Ioku K. Influence of surface microstructure on the reaction of the active ceramics in vivo. J Mater Sci Mater Med 1998;9:381–4.
[22] Nakamura S, Kobayashi T, Yamashita K. Numerical osteobonding evaluation of electrically polarized hydroxyapatite ceramics. J Biomed Mater Res A 2004; 68:90–4.
[23] Itoh S, Nakamura S, Kobayashi T, Shinomiya K, Yamashita K, Itoh S. Effect of electrical polarization of hydroxyapatite ceramics on new bone formation. Calcif Tissue Int 2006;78:133–42.
[24] Kawachi G, Sasaki S, Nakahara K, Ishida EH, Ioku K. Porous apatite carrier prepared by hydrothermal method. Key Eng Mater 2006;309–311: 935–8.

Key Engineering Materials Vols. 396-398 (2009) pp 253-256
online at http://www.scientific.net

Online available since 2008/Oct/21

Osteoconductivity of hydrothermally synthesized beta-tricalcium phosphate composed of rod-shaped particles under mechanical unloading

Yoshinori Gonda[1, 2, a], Koji Ioku[3, b], Takatoshi Okuda[2, c], Yasuaki Shibata[1, d], Masanobu Kamitakahara[3, e], Giichiro Kawachi[4, f], Ikuho Yonezawa[2, g], Hisashi Kurosawa[2, h] and Tohru Ikeda[1, i]

[1]Division of Oral Pathology and Bone Metabolism, Department of Developmental and Reconstructive Medicine, Nagasaki University Graduate School of Biomedical Sciences, 1-7-1 Sakamoto, Nagasaki 852-8588, Japan

[2]Department of Orthopedic Surgery, School of Medicine, Juntendo University, 2-1-1 Hongo, Tokyo 113-8421, Japan

[3]Graduate School of Environmental Studies, Tohoku University, 6-6-20Aramaki, Aoba-ku, Sendai 980-8579, Japan

[4]Department of Crystalline Materials Science, Graduate School of Engineering, Nagoya University, Furo-cyo, Chikusa-ku, Nagoya 464-8603, Japan

[a]gondayoshinori@mac.com, [b]ioku@mail.kankyo.tohoku.ac.jp, [c]o-kun@med.juntendo.ac.jp, [d]siva@nagasaki-u.ac.jp, [e]kamitaka@mail.kankyo.tohoku.ac.jp, [f]kawachi@apchem.nagoya-u.ac.jp, [g]yoza@med.juntendo.ac.jp, [h]kuro@med.juntendo.ac.jp, [i]tohrupth@net.nagasaki-u.ac.jp

Keywords: Beta tricalcium phosphate, Bone graft, Unloading

Abstract. Spherical beta-tricalcium phosphate (β-TCP) granules synthesized using a unique dropping slurry method expressed good osteoconductivity with prominent bone apposition and bioresorbability when implanted into the rat femur (Gonda et al., *Key Eng. Mater.* 361-363:1013-1016, 2008). The spherical β-TCP granules were implanted into the bone defect created in the distal end of the right femur of each 8-week-old female Wistar rat. To analyze performance of the spherical β-TCP granules as bone substitute in the bone with reduction in osteogenic potential, the right sciatic neurectomy was performed after implantation and the right hind limb was kept unloaded for 2 weeks before euthanization. Four weeks after implantation, some spherical β-TCP granules with resorption in part were surrounded by newly formed bone. Eight and 12 weeks after implantation, most of the residual β-TCP granules were embedded in newly formed bone, and total volume of the implant and newly formed bone was more than the other portions of the bone or the bone of control animals. Osteoclast activity in the implanted area was also higher than the other portions of the bone or the bone of control animals. Replacement of the intraosseous residual β-TCP granules for bone progressed at 12 weeks after implantation compared to those at 8 weeks after implantation. These data suggested that the spherical β-TCP granules stimulated osteogenesis and osteoclast activity of the unloaded bone.

Introduction

Beta-tricalcium phosphate (β-TCP) has been used clinically as a bioresorbable bone substitute. In addition to the porosity and the structure of micro and macro pores, microstructure of the particles composing the material has also been shown to be associated with the bioresorbability [1]. We have shown that the cylindrical block of β-TCP composed of unique rod-shaped particles behaved differently from the same-shaped block of conventional β-TCP composed of non rod-shaped particles when implanted into rabbit femurs, and proposed the hypothesis that bioresorbability of the bone substitute affected the metabolism of the subsequently formed bone tissue [2]. Previously, we also have developed spherical granules of β-TCP using a new unique method [3]. After implantation into rat femurs, both spherical β-TCP granules composed of rod-shaped particles produced by hydrothermal method and β-TCP granules composed of non rod-shaped particles revealed good osteoconductivity. Total volume of the newly formed bone and implant was similar

between animals implanted β-TCP composed of rod-shaped particles and animals implanted β-TCP composed of non rod-shaped particles, but the volume of newly formed bone/total volume of newly formed bone and implant was higher in the animals implanted β-TCP granules composed of rod-shaped particles than the animals implanted β-TCP granules composed of non rod-shaped particles [4]. In this study, we analyzed osteoconductivity and bioresorbability of spherical β-TCP granules composed of rod-shaped particles in the bone with reduction in osteogenic potential induced by mechanical unloading [5].

Materials and Methods

Production of Spherical β-TCP Granules: Alpha-TCP powder was mixed and kneaded with gelatine, and dropped into stirring oil bath heated at 80°C. Then, the bath was chilled on ice and formed spherical α-TCP granules. The granules were separated from the oil, rinsed, and served for hydrothermal treatment to produce spherical β-TCP granules composed of rod-shaped particles [6]. The size was ranged from 0.5 to 0.6 mm in diameter. The synthesized spherical β-TCP granules were analyzed by X-ray diffractometry, and no phase other than β-TCP was detected. Rod-shaped particles of spherical β-TCP granules were confirmed using a scanning electron microscope.

Animal Experiments: Eight-week-old female Wistar rats were anesthetized, a bone defect 2 mm in diameter and 3 mm in depth was created in distal end of the right femur of each animal, 30 mg of β-TCP granules were implanted and the wound portion was sutured. Operated animals without implantation of β-TCP granules were used as a control. The right sciatic neurectomy was performed 2 weeks before euthanization. Four, 8 and 12 weeks after implantation, animals were euthanized and operated bones were resected. Undecalcified bone tissue sections were made from the resected bones and analyzed histologically. Rearing of these animals and animal experiments were performed following the Guidelines of Animal Experimentation of Nagasaki University.

Results and Discussion

Right tibiae 2 weeks after sciatic neurectomy revealed growth retardation and decreased bone mass compared to the left tibiae without neurectomy, and unloading of the right limb was confirmed. In the operated right femur, regeneration of the non-critical sized bone defect in the unloaded bone was apparently delayed compared to the loaded bone (data not shown). Four weeks after implantation, newly formed bone appeared around the partially resorbed implant. Bone regeneration occurred from marginal region of the bone defect and implanted β-TCP granules in the marginal region of operated area were already surrounded by newly formed bone. In central region of the operated area, connective tissue still remained (Fig. 1A). Marginal region of the bone defect of control animals was partly regenerated, but most part of the defect remained and was filled with connective tissue (Fig. 1B). At 8 weeks after implantation, prominent bone formation was seen in and around the implant in contrast to the control (Fig. 1C, D). Greater numbers of tartrate-resistant acid phosphatase-positive cells were present around the implant than those in the other portions of the bone and in the control bone (data not shown). At 12 weeks after implantation, histological findings were similar to those at 8 weeks after implantation (Fig. 1E). Total volume of the implant and newly formed bone was much more than the other portions of the bone in the animals 8 weeks and 12 weeks after implantation. In the control bone, the created bone defect was mostly regenerated at 8 weeks after operation, the bone defect were mostly regenerated. At 12 weeks after operation the cancellous bone which was formed in the created bone defect was indistinguishable from surrounding slender cancellous bone under mechanical unloading (Fig. 1D, F). Under polarizing microscope, refringence of lamellar structure of bone enables to distinguish implanted β-TCP granules from bone tissue. As shown in Fig. 2A, considerable amount of β-TCP embedded in the bone was seen in the specimens 8 weeks after implantation. At 12 weeks after implantation, part of the embedded β-TCP granules was replaced by bone and newly formed bone was seen within the implanted granules (Fig. 2B). Total volume

of newly formed bone in the animals implanted with β-TCP granules was significantly higher than that in control animals created the bone defect. These data suggested that the spherical β-TCP granules stimulated osteogenesis and osteoclast activity in the unloaded bone. In addition, it was also suggested that replacement of the intraosseous residual β-TCP granules for bone occurred in the suppressive osteogenetic conditionunder the mechanical unloading.

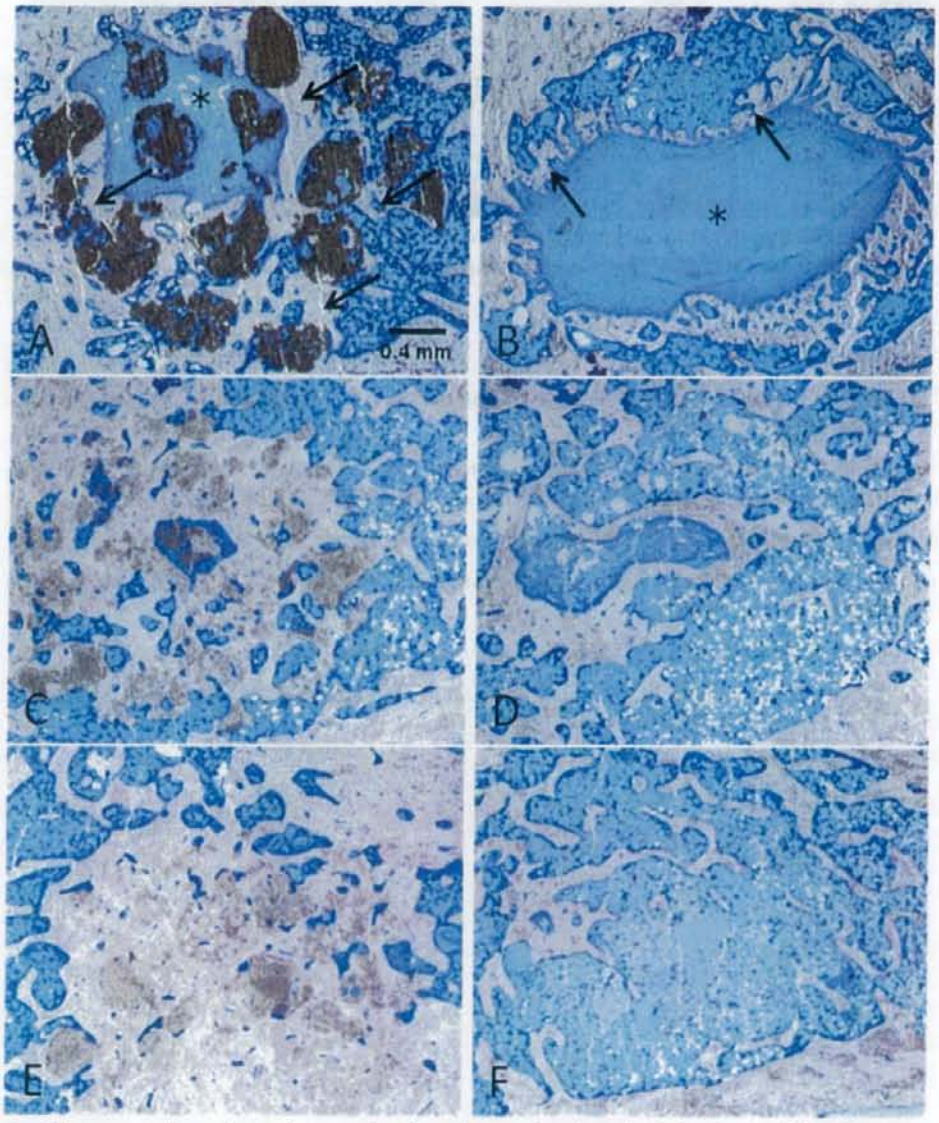

Fig. 1 Representative photomicrograph of specimens implanted with spherical β-TCP granules (A, C, E) and control specimens without implantation into the bone defects (B, D, F). Specimens 4 weeks (A, B), 8 weeks (C, D) and 12 weeks after operation (E, F) were stained with Giemsa's method. For all specimens, sciatic neurectomy was performed 2 weeks before sampling for histological analyses. Arrows indicate newly formed bone in marginal region. Asterisks (*) represent connective tissue in the bone defect.

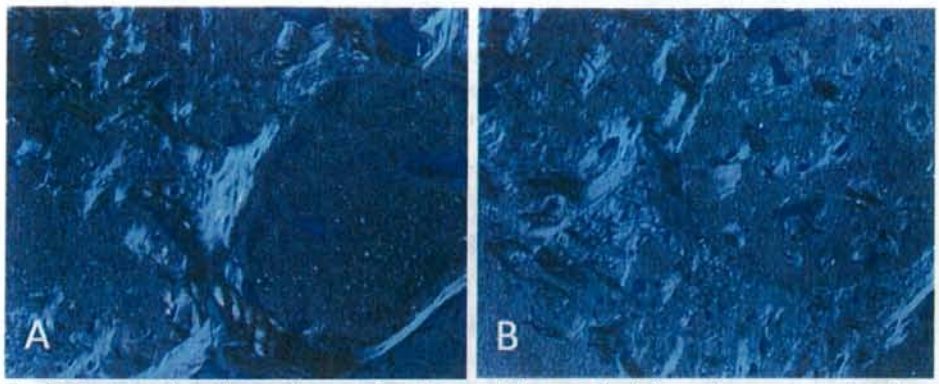

Fig. 2 Representative photomicrographs observed by a polarizing microscope. Specimens 8 weeks (A) and 12 weeks (B) after implantation of spherical β-TCP granules.

References

[1] H. Yokozeki, T. Hayashi, N. Nakagawa, H. Kurosawa, K. Shibuya and K. Ioku. *J. Mater. Sci. Mater. Med.* **9**:381-384. (1998)

[2] T. Okuda, K. Ioku, I. Yonezawa, H. Minagi, G. Kawachi, Y. Gonda, H. Murayama, Y. Shibata, S. Minami, S. Kamihira, H. Kurosawa and T. Ikeda. *Biomaterilas* **28**:2612-2621. (2007)

[3] K. Ioku, G. Kawachi, S. Sasaki, H. Fujimori, S. Goto. *J. Mater. Sci.* **41**:1341-1344. (2006)

[4] Y. Gonda, K. Ioku, T. Okuda, G. Kawachi, I. Yonezawa, H. Kurosawa, T. Ikeda. *Key Eng. Mater.* **361-363**:1013-1016. (2008)

[5] M. Weinreb, G. A. Rodan, D. D. Thompson. *Bone* **10**:187-194. (1989)

[6] K. Ioku, M. Kamitakahara, G. Kawachi, Y. Gonda, T. Okuda, I. Yonezawa, H. Kurosawa, T. Ikeda, *Key Eng. Mater.* **361-363**:989-992. (2008)

Bioceramics 21
doi:10.4028/www.scientific.net/KEM.396-398

Osteoconductivity of Hydrothermally Synthesized Beta-Tricalcium Phosphate Composed of Rod-Shaped Particles under Mechanical Unloading
doi:10.4028/www.scientific.net/KEM.396-398.253

Key Engineering Materials Vols. 396-398 (2009) pp 645-648
online at http://www.scientific.net

Online available since 2008/Oct/21

Calcium Phosphate Porous Materials with Unique Microstructures

Koji Ioku[1, a], Masanobu Kamitakahara[1, b] Noriaki Watanabe[1, c], Osamu Kawaguchi[1], Setsuaki Murakami[1], Tohru Ikeda[2, d]

[1]Graduate School of Environmental Studies, Tohoku University
Aoba 6-6-20, Aramaki, Aoba-ku, Sendai 980-8579, Japan

[2]Division of Oral Pathology and Bone Metabolism
Department of Developmental and Reconstructive Medicine
Nagasaki University Graduate School of Biomedical Sciences
1-7-1 Sakamoto, Nagasaki 852-8588, Japan

[a]ioku@mail.kankyo.tohoku.ac.jp, [b]kamitaka@mail.kankyo.tohoku.ac.jp,
[c]watanabe@ehtp.kankyo.tohoku.ac.jp, [d] tohrupth@net.nagasaki-u.ac.jp

Keywords: Hydroxyapatite, Calcium phosphate, TCP, Granule, Hydrothermal

Abstract. Three types of calcium phosphate porous materials were prepared by the applied hydrothermal method. One of them was non-stoichiometric hydroxyapatite (HA) with calcium deficient composition and the others were β-tricalcium phosphate (β-TCP) and HA/β-TCP bi-phase material. Granules with several millimeter in size of calcium deficient HA, β-TCP and HA/β-TCP could be prepared. These granules with porosity over 70 % were composed of rod-shaped particles with aspect ratio about 10. Rod-shaped particles were locked together to make sub-micro-sized pores of about 0.1 to 0.5 μm in size. These materials must be suitable for the bone graft materials and as the scaffolds of cultured bone.

Introduction

Porous materials of hydroxyapatite (HA: $Ca_{10}(PO_4)_6(OH)_2$) and β-tricalcium phosphate (β-TCP : β-$Ca_3(PO_4)$) with large size pores which allow cells to enter easily into them are currently used as bone graft substitutes [1-5]. They have been known to be biocompatible and osteoconductive [6]. Several previous studies have also confirmed that HA is a stable material *in vivo* [7-9] and β-TCP is more biodegradable as the implant material than HA [10-12].

The authors reported that sub-micro-sized pores of β-TCP with about 0.1-0.5 μm in size were significantly important for bio-resorption in bones [13]. In addition, the microstructure of materials influenced the bone formation [14, 15]. Therefore, microstructure of materials such as particle shape, size and sub-micro-sized pores should be controlled for bone graft materials.

The present paper deals with the preparation of HA, β-TCP and HA/β-TCP bi-phase porous materials with unique microstructures by applied hydrothermal methods.

Experimental

Preparation of Calcium Phosphate Materials. Powders of α-tricalcium phosphate (α-$Ca_3(PO_4)_2$: α-TCP) and gelatin were used as the starting materials. The slurry of α-TCP with gelatin was prepared as aqueous solution at room temperature. To remove bubbles, the slurry was kept under vacuum condition. The slurry was dropped into liquid nitrogen to form the spherical shape. To remove gelatin and to keep the crystal phase of α-TCP, the resultant spherical particles with several millimeter in size were heated at 1200 °C for 10 min. in air. They were put in sealed vessels with pure water and then treated hydrothermally at the temperatures from 120 °C to 180 °C under saturated water vapor pressure for the periods from 3 h to 24 h.

Characterization. The produced phases were identified by powder X-ray diffractometry with graphite-monochromatized CuKα radiation, operating at 40 kV and 40 mA (XRD; RINT 2200V/PC-LR, Rigaku Japan). The samples prepared were dissolved in 0.1 mol · dm^{-3} nitric acid, and then the chemical composition of them was analyzed by inductively coupled plasma spectrometer (ICP-MS; Seiko Instruments, SPQ 9000S, Japan). The microstructure of specimens was observed by scanning electron microscope (SEM; S-4100, Hitachi, Japan). Pore volume and distribution of pore diameter were measured by mercury intrusion porosimetry (MIP; Poremaster 33P, Quantachrome, USA). Specific surface area of samples was measured by a nitrogen gas sorption method of BET.

Results and Discussion

Porous granules of calcium deficient HA. Spherical mixture of α-TCP and gelatin were obtained after dropping slurry into liquid nitrogen. Gelatin was observed among the particles of α-TCP. After heating at 1200 °C for 10 min, gelatin was burned out and no other phases than α-TCP were revealed by XRD. The XRD pattern of the sample after hydrothermal treatment is showing high crystallinity of HA and the non-existence of phases other than HA. Microstructure designed HA granules of about 1 mm to 3 mm in size could be prepared by hydrothermal vapor exposure method at the temperatures from 120 °C to 180 °C under saturated vapor pressure of pure water. The granular HA was composed of rod-shaped crystals of about 10 μm in length with the mean aspect ratio of 10. Rod-shaped HA crystals were locked together to make sub-micro-sized pores of about 0.1 μm in size. It was non-stoichiometric HA with calcium deficient composition of Ca/P<1.60 according to ICP-MS analysis. The size of granules depended on the state of dropping. Specific surface area of samples was about 10 m^2/g. Microstructure designed granules of calcium deficient HA must be suitable for bone graft materials and for scaffolds of cultured bone.

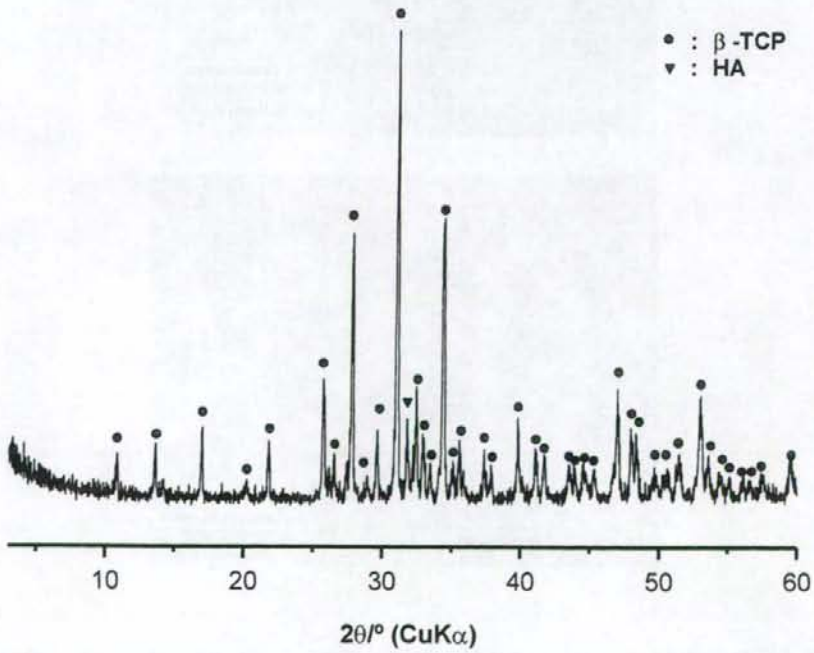

Figure 1 XRD of HA/β-TCP granules prepared from calcium deficient HA.

Porous granules of β-TCP and HA/β-TCP. Calcium deficient HA tends to decompose into tricalcium phosphates by heating [16, 17]. Thus, porous materials of β-tricalcium phosphate (β-$Ca_3(PO_4)_2$: β-TCP) were obtained from the porous materials of calcium deficient HA with Ca/P ratio of 1.50 by heating it at 900 ℃ for 3 h in air, according to decomposition of calcium deficient HA. This porous β-TCP had almost the same micro-structure in comparison with the porous HA before heating. The porous β-TCP was composed of rod-shaped particles with about 10 μm in length, and it had almost same porosity as the samples before heating. The mean diameter of sub-micro-sized pore of β-TCP materials was slight larger than that of HA, the value was about 0.2 μm in size. Porous β-TCP with much amount of sub-micro-sized pores prepared in this study should be more bio-degradable than the conventional materials of β-TCP.

Porous HA/β-TCP bi-phase granules with the same unique microstructures mentioned above were prepared from calcium deficient HA with Ca/P ratio over1.50 by heating it at 900 ℃ for 3 h in air. One example of XRD patterns was shown in Figure 1. The porous granules of HA/β-TCP were composed of rod-shaped particles with much amount of sub-micro-sized pores (Figure 2). The mixture ratio of HA and β-TCP could be controlled by controlling the Ca/P ratio of calcium deficient HA.

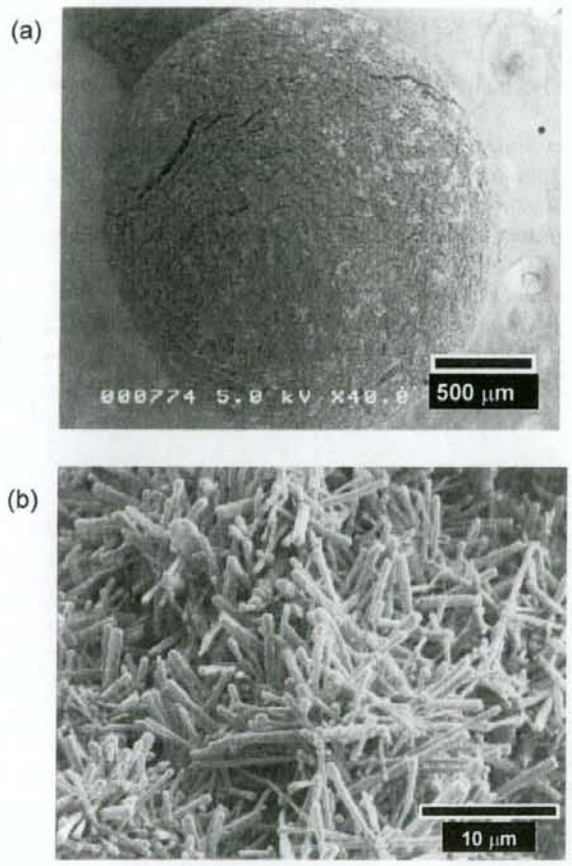

Figure 2 Photographs of SEM for the HA/β-TCP granule. The granule (a) was composed of rod- shaped particles (b). The mixture ratio of HA and β-TCP was controllable.

Summary

The results described in this paper allow to drawing the following conclusions.

(1) Porous granules of calcium deficient HA with over 70 % porosity were prepared by the hydrothermal method. These granules were composed of rod-shaped crystals of about 10 μm in length. These materials had the sub-micro-sized pores of about 0.1 μm in size.

(2) Porous granules of β-TCP and HA/β-TCP were prepared from the calcium deficient HA by heating at 900 ℃ for 3 h in air. These granules were composed of rod-shaped particles of about 10 μm in length, and had much amount of sub-micro-sized pores. The mean diameter of sub-micro-sized pores of these materials was slight larger than that of HA granules, the value was about 0.2 μm in size.

(3) The mixture ratio of HA and β-TCP for HA/β-TCP granules was controllable by controlling the Ca/P ratio of calcium deficient HA.

References

[1] R.A. Finn, W.H. Bell and J.A. Brammer: J. Max. Fac. Surg., **8**, 217-227 (1980).

[2] R.M. Meffert, J.R. Thomas, K.M. Hamilton and C.N. Brownstein: J. Periodontal, **56**, 63-73 (1985).

[3] D.J. Sartoris, D.H. Gershuni, W.H. Akeson, R.E. Holmes and D. Resnick: Radiology, 159, 133-137 (1986).

[4] K. Ioku: J. Soc. Inorg. Mater. Japan, **3**, 412-418 (1996).

[5] K. Ioku: J. Soc. Inorg. Mater. Japan, **8**, 153-159 (2001).

[6] M. Jarcho: Clin. Orthop., 157, 259-278 (1981).

[7] K. Ioku, K. Yanagisawa, N. Yamasaki, H. Kurosawa, K. Shibuya, H. Yokozeki and T. Hayashi: Bio-Med. Mater. Eng., **3**, 137-145 (1993).

[8] K. Ioku, H. Kurosawa, K. Shibuya, H. Yokozeki and T. Hayashi: *Bioceramics Vol.7*, Ed. by H. Andersson and A. Yli-Urpo, Butterworth-Heinemann, (1994) pp.97-102.

[9] K. Ioku, S. Goto, H. Kurosawa, K. Shibuya, H. Yokozeki, T. Hayashi and T. Nakagawa: *Bioceramics Vol.9*, Ed. by T. Kokubo, T. Nakamura and F. Miyaji, Elsevier Science, Japan (1996) pp.201-204.

[10] H.U. Cameron, I. Macnab and R.M. Pilliar, J. Biomed. Mater. Res., **11**, 179-186 (1977).

[11] S.F. Hulbert, F.A. Young, R.S. Mathews, J.S. Klawitter, C.D. Talbert and F.H. Stelling: J. Biomed. Mater. Res., **4**, 433-456 (1970).

[12] K. Ioku, S. Goto, H. Kurosawa, K. Shibuya, H. Yokozeki, T. Hayashi and T. Nakagawa: Phosp. Res. Bull., **7**, 29-34 (1997).

[13] H. Yokozeki, T. Hayashi, T. Nakagawa, H. Kurosawa, K. Shibuya and K. Ioku: J. Mater. Sci.: Mater. Med., **9**, 381-384 (1998).

[14] T. Okuda, K. Ioku, I. Yonezawa, H. Minagi, G. Kawachi, Y. Gonda, H. Murayama, Y. Shibata, S. Minami, S. Kamihira, H. Kurosawa, T. Ikeda: Biomaterials, **28**, 2612-2621 (2007).

[15] T. Okuda, K. Ioku, I. Yonezawa, H. Minagi, Y. Gonda, G. Kawachi, M. Kamitakahara, Y. Shibata, H. Murayama, H. Kurosawa, T. Ikeda, Biomaterials, **29**, 2719-2728 (2008).

[16] K. Ioku, T. Murakami, Y. Ikuma and M. Yoshimura: J. Ceram. Soc. Japan, Int. Edition, **100**, 1001-1005 (1992).

[17] K. Ishikawa, P. Ducheyne and S. Radin, J. Mater. Sci.: Mater. Med., **4**, 165-168 (1993).

Bioceramics 21
doi:10.4028/www.scientific.net/KEM.396-398

Calcium Phosphate Porous Materials with Unique Microstructures
doi:10.4028/www.scientific.net/KEM.396-398.645

Available online at www.sciencedirect.com
ScienceDirect
Mutation Research 638 (2008) 48–55
Fundamental and Molecular Mechanisms of Mutagenesis
www.elsevier.com/locate/molmut
Community address: www.elsevier.com/locate/mutres

Mutagenic radioadaptation in a human lymphoblastoid cell line

Fumio Yatagai [a,*], Yukihiro Umebayashi [a], Masamitsu Honma [b], Kaoru Sugasawa [c], Yuko Takayama [a], Fumio Hanaoka [d]

[a] *Advanced Development and Support Center, The Institute of Physical and Chemical Research (RIKEN), Saitama 351-0198, Japan*
[b] *Division of Genetics and Mutagenesis, National Institute of Health Sciences, Tokyo 158-8501, Japan*
[c] *Genome Damage Response Research Unit, The Institute of Physical and Chemical Research (RIKEN), Saitama 351-0198, Japan*
[d] *Graduate Program, Frontiers in Biosciences, Osaka University, Osaka 565-0871, Japan*

Received 6 April 2007; received in revised form 15 August 2007; accepted 22 August 2007
Available online 1 September 2007

Abstract

We investigated the mutagenic radioadaptive response of human lymphoblastoid TK6 cells by pretreating them with a low dose (5 cGy) of X-rays followed by a high (2 Gy) dose 6 h later. Pretreatment reduced the 2-Gy-induced mutation frequency (MF) of the *thymidine kinase* (*TK*) gene (18.3×10^{-6}) to 62% of the original level (11.4×10^{-6}). A loss of heterozygosity (LOH) detection analysis applied to the isolated TK^- mutants revealed the mutational events as non-LOH (resulting mostly from a point mutation in the *TK* gene), hemizygous LOH (resulting from a chromosomal deletion), or homozygous LOH (resulting from homologous recombination (HR) between chromosomes). For non-LOH events, pretreatment decreased the frequency to 27% of the original level (from 7.1×10^{-6} to 1.9×10^{-6}). cDNAs prepared from the non-LOH mutants revealed that the decrease was due mainly to the repression of base substitutions. The frequency of hemizygous LOH events, however, was not significantly altered by pretreatment. Mapping analysis of chromosome 17 demonstrated that the distribution and the extent of hemizygous LOH events were also not significantly influenced by pretreatment. For homozygous LOH events, pretreatment reduced the frequency to 61% of the original level (from 5.1×10^{-6} to 3.1×10^{-6}), reflecting an enhancement in HR repair of DNA double-strand breaks. Our findings suggest that the radioadaptive response in TK6 cells follows mainly from mutations at the base-sequence level, not the chromosome level.

Keywords: Adaptive response; TK6 cells; LOH detection system

1. Introduction

An adaptive cellular response occurs when a mild stress applied before a challenging treatment with a DNA-damaging agent decreases the detrimental effects of the challenge. In radioadaptation, as it is usually defined, exposure to a low dose of ionizing radiation (IR) provides some protection against a high dose. Radioadaptation was first reported by Olivieri et al. [1], who showed that radiation delivered by labeling human lymphocytes with tritiated thymidine causes a decrease in the frequency of chromosomal aberrations induced by subsequent exposure to 15 Gy of IR. That discovery stimulated a series of studies in human lymphocytes and various mammalian cell lines (for review, see refs. [2,3]) and suggested that the adaptive response is an important defense mechanism, especially against low doses of IR. The molecular mechanisms involved, however, remain largely unknown [4–8], and cellular

* Corresponding author. Tel.: +81 48 467 9710; fax: +81 48 462 1426.
E-mail address: yatagai@postman.riken.go.jp (F. Yatagai).

0027-5107/$ – see front matter © 2007 Elsevier B.V. All rights reserved.
doi:10.1016/j.mrfmmm.2007.08.014

responses such as the bystander effect, genetic instability and hyper-radiosensitivity seem tightly related to the adaptive response in a specific low-dose region. One of the hot subjects in recent adaptive response studies is the expression of the genes involved in the mechanism [8–10]. Another is the relationship between the adaptive response and the bystander effect [11–15]. In mammalian cells, for example, bystander mutagenesis may be suppressed by an adaptive response [11].

Following the report by Olivieri et al., reduced induction of both micronuclei and sister chromatid exchanges was shown in Chinese hamster V79 cells pre-exposed to low doses of γ-rays or ^{3}H β-rays [16]. Subsequent studies reported similar radioadaptive responses, such as reduced mutation frequencies in human lymphocytes [17], mouse SR-1 cells [18] and human–hamster hybrid A_L cells [19], an altered mutation spectrum in human–hamster hybrid A_L cells [19], reduced micronucleus frequencies in human lymphocytes [5] and mouse embryo cells [20], and reduced deletions and rearrangements in human lymphoblast cells [21]. The mechanism underlying those radioadaptations may have been the induction of an efficient chromosome repair system by the priming radiation dose, and in fact, the efficiency of DNA double-strand break (DSB) repair in Chinese hamster V79 cells exposed to γ-rays is enhanced by a priming exposure of 5 cGy of γ-rays [22]. Furthermore, DSBs with either blunt or staggered ends, created by restriction enzymes, induce the adaptive response [3].

The human lymphoblastoid TK6 cell line, isolated by Skopek et al. [23], is heterozygous at the *thymidine kinase* (*TK*) locus. Honma's laboratory developed a loss of heterozygosity (LOH) detection system that can be used for molecular analysis of *TK* mutations as well as for detecting alterations at the chromosome level [24,25]. Using that methodology, we were able to detect IR effects at doses as low as 10 cGy [26–28]. Irradiation of TK6 cells with 10 cGy of X-rays clearly demonstrated radiation-specific types of LOH events or interstitial deletions in chromosome 17 [26]. We also observed more efficient induction of such events after 10 cGy irradiation with an accelerated carbon-ion (135 MeV/u) beam [27], and this was apparent in frozen cells exposed to the same carbon-ion beam [28]. These results strongly suggest that the interstitial deletions were the result of end-joining repair of IR-induced DSBs.

Because the radiation-sensitive LOH analysis system in TK6 cells is effective for detecting the fate of radiation-induced DNA double-strand breaks (DSBs), we use it here to see if the adaptive response could produce measurable changes in IR-induced genetic alterations. The results we obtained were not completely expected, but are interesting.

2. Materials and methods

2.1. Cell culture and adaptive treatment

The methodologies for the detection of *TK*-deficient mutants and the materials and methods used for cell culture and growth have been previously reported [26]. Briefly, TK6 cells were incubated in RPMI1640 medium supplemented with HAT to eliminate pre-existing TK^- deficient mutants. The cells were then resuspended in fresh normal medium, and 6 ml cell suspension was dispensed into 6-cm diameter Petri dishes. The cells were pretreated ("primed") with 2.5, 5 or 10 cGy of X-rays (250 kVp) at a rate of 10 cGy/min, and placed in a 5% CO_2 humidified incubator. The cell concentration was adjusted to 8×10^5 cells/ml at the end of the post-irradiation incubation period of 1.5, 3, 6, 9 or 12 h. The cells were then challenged with 2 Gy X-rays (250 kVp) at 1 Gy/min. Non-primed irradiated cells treated in the same manner as the primed cells served as controls.

2.2. Survival assay and TK mutation assay

To determine the surviving fraction of the challenged cells, we measured the plating efficiency (PE) immediately after irradiation using the limiting dilution method. For mutation expression, we incubated the cells with non-selecting RPMI1640 medium for about 60 h following the X-ray challenge. We measured the PE of incubated cells similarly, determining the *TK* mutation frequency. To select TK^- mutant clones, we seeded incubated cells into 96-well plates at 4×10^4 cells per well in RPMI1640 medium containing 4 μg/ml trifluorothymidine (TFT); we harvested the normally growing clones after 2 weeks and the slow growing clones after 4 weeks.

2.3. Determination of optimum irradiation conditions for mutagenic adaptation

To determine the optimum conditions for evoking the mutagenic radioadaptive-response, we tested the MF induced by 2 Gy at 0, 1.5, 3, 6, 9 and 12 h after a priming dose of 10 cGy, selected the optimum interval time, and then tested the MF induced by 2 Gy at that interval time after priming doses of 0, 2.5, 5 and 10 cGy.

2.4. LOH analysis of TK^- mutants

Fig. 1 illustrates how we classified TK^- mutants. We first determined *TK* LOH by PCR analysis of exons 4 and 7 [29]. If the PCR products of both were similar to those of the parental *TK* heterozygous cells, we classified the mutant